MEASUREMENT OF THE ELECTRON TEMPERATURE IN A METALLIC COPPER USING ULTRAFAST LASER-INDUCED BREAKDOWN SPECTROSCOPY

Mohamed Fikry,[1,2] **Walid Tawfik,**[3*] **and Magdy Omar**[1]

[1] *Department Physics, Faculty of Science*
Cairo University, Cairo, Egypt

[2] *Egypt Nanotechnology Center (EGNC)*
Cairo University, Cairo, Egypt

[3] *National Institute of Laser Enhanced Sciences (NILES)*
Cairo University, Cairo, Egypt

*Corresponding author e-mail: walid_tawfik @ niles.edu.eg

Abstract

In this paper, we provide the laser-induced breakdown spectroscopic (LIBS) analysis of copper under the action of the ultrafast picosecond Nd:YAG laser and the specifications calculated from the electron temperature of plasma generated by the fundamental (1064 nm), second (532 nm), third (355 nm), and fourth (266 nm) laser harmonics. In this work, a laser pulse energy of 60 mJ $\pm 5\%$ with a duration of 170 ps, a beam diameter of $\sim 0.5 \pm 0.1$ mm, and a laser intensity $1.79 \cdot 10^{11}$ W/cm^2 $\pm 8\%$ for a single shot was applied. The electron temperature is measured using three spectral lines of neutral copper (Cu I) at 515.3, 521.8, and 522.0 nm, according to the Boltzmann plot model where the local thermodynamic equilibrium (LTE) conditions were assumed. The electron temperature values observed are 13422, 15152, 16605, and 17783 K for laser wavelengths of 266, 355, 532, and 1064 nm, respectively. The experimental analysis reveals that the plasma electron temperature rises with the laser wavelength. Variations in the mass ablation rate, inverse Bremsstrahlung absorption, and photoionization with the laser wavelength variation allow us to explore the interaction dynamics. The results obtained allow for variation of the generated plasma electron temperature by guiding the picosecond pulse wavelengths; the later may allow for controlling plasma interactions, which can be applied in plasma spectroscopy of material science.

Keywords: ultrafast picosecond laser pulse, laser-induced breakdown spectroscopy (LIBS), copper plasma, electron temperature, Boltzmann plot, local thermodynamic equilibrium (LTE).

1. Introduction

A material breakdown can be generated by the plasma interaction, which created significant change in a matter temperature to overcome the binding electrostatic forces between its electrons and nuclei [1]. Subsequently, very hot gas is therefore collected of a mixture of neutral atoms, electrons, and ions [2]. Plasma breakdown spectroscopy is an important diagnostic method in plasma physics and technology. The plasma has two main categories, according to its temperature – the hot plasma with temperature T_p ranged from 10^6 K to 10^8 K and the cold plasma with temperature ranged from 10^3 K to 10^4 K [3].

1071-2836/20/4105-0484 ©2020 Springer Science+Business Media, LLC

Using a laser beam to induce material breakdown by focusing a high-energy laser pulse on any target material (solid, liquid or gas) is one of the essential plasma generation methods. The created radiation can lead to quick local heating, powerful evaporation, and degradation of the material at the focal point [4]. The interaction between the laser beam and the material depends on the mechanical, physical, and chemical features of the target, as well as on the properties of the laser [5].

Laser-induced breakdown irradiates emission spectra of various types, mostly extent from ultraviolet to visible and infrared regions. The technique based on the spectroscopic analysis of laser-produced breakdown optical emission is known as laser-induced breakdown spectroscopy (LIBS) [6]. The LIBS technique is suitable for fast on-line basic assessment of all material phases used to estimate the ratio target's impurity components with conventional calibration and empiric calibration-free methods [7].

Recently, ultrafast (ranged from picosecond to femtosecond) laser pulses became an interesting topic of research within laser pulse applications [8]. The studies of picosecond lasers include optical coherence tomography, new solutions for optical communications, and ultrashort laser pulse management. The ultrafast laser processing of materials provides various advantages over conventional procedures – a quick, accurate, and versatile technique, due to the electron–phonon interaction and quicker vaporization of the target material than the energy transfer to the surrounding areas [9]. For picosecond laser pulses, it has been previously shown that they are able to induce breakdown ablation with reduced heat-affected zone and less heat dissipation compared to nanosecond laser-pulse ablation [10].

Some scientists have studied the effect of the laser wavelength on the laser-induced breakdown spectroscopy parameters. In 2002, Abdellatif and Imam studied the laser-plasma parameters achieved by the nanosecond Nd:YAG laser at various laser wavelengths (1064, 532, and 355 nm) with different laser pulse energies (60, 100, and 500 mJ) for aluminum plates at different focusing lengths [11]. They determined that the maximum value of the electron temperature T_e was found at a certain distance away from the target surface depending on the laser wavelength, whereas the electron concentration N_e reaches its highest value near the target surface. In 2006, Fornarini et al. studied a range of fluxes $50-250$ J/cm^2 of Nd:YAG laser with wavelengths of 1064 and 355 nm and with a pulse duration of 8 ns basing on the analytical outcomes acquired from the use of LIBS diagnostics of bronze plasma [12]. They inferred that more limited thermal effects are expected if a laser with a shorter wavelength is considered.

In 2015, Aberkane et al. determined the effect of 50 mJ Nd:YAG laser wavelengths 1064, 532, and 355 nm at 7, 9, and 10 ns pulse durations in the air at atmospheric pressure on the correlation between T_e and surface hardness of Fe–V–C metallic alloys [13]. They decided that the surface hardness measurement using LIBS is more efficient for the excitation laser with IR wavelength than with UV one. In 2019, the ultrafast femtosecond laser with a pulse wavelength of 800 nm, a pulse duration of 50 fs, and 1.9 mJ laser energy was used by Xu et al. to generate a high T_e and low N_e plasma with strong spectral intensity by changing the distance between the focusing lens and the sample surface in the LIBS configuration [14]. They found that the plasma with high T_e and low N_e can be used to improve the spectral resolution of LIBS.

In this work, we aim to apply a picosecond laser-induced breakdown spectroscopy to investigate the created copper-plasma spectrum. We study the LIBS spectra lines in the visible region and the effect of different laser wavelengths on the electron temperature in the plasma plume. We intentionally try to control a specific range of the plasma temperature by varying the wavelength of a picosecond laser pulse.

2.　Methodology

In the current experiment, the plasma was produced by focusing an ultrafast picosecond Q-switched Nd:YAG laser on a solid sample of a pure metal copper disk (K. J. Lasker Ltd., USA, a purity of 99.99%) with a thickness of 0.25 cm and a diameter of 3 cm. The experimental setup was shown and described previously [15], except the fact that the nanosecond ND:YAG laser is replaced by a 170 ps Q-switched Nd:YAG laser with four wavelengths: 1064, 532, 355, and 266 nm. This laser can deliver pulse energy of 60 mJ $\pm 5\%$ at repetition rate of 1–5 Hz and laser intensity of $1.79 \cdot 10^{11}$ W/cm^2 $\pm 8\%$ under the atmospheric pressure. The laser pulse was monitored via a laser power meter (Model 11 Maestro, Standa LTD, Lithuania), then focused by a plane–convex quartz lens with a 150 mm focal length on the Cu disk target with a spot size of $\sim$0.5 $\pm$0.1 mm to produce a plasma plume.

The copper target was placed on the $x - y$ scanning stage to provide refreshing of the sample's material surface for each laser pulse to minimize errors. A plane–convex quartz lens with a focal length of 100 mm was adjusted to the center of the plasma plume to collect the plasma emission at the 90° position to the laser axis. The collected emission was then transferred to an Ocean Optics spectrometer (HR4000 UV–NIR, $200 - 1100$ nm) using an optical fiber with 400 μm core diameter. The integration time was considered to be optimum at 10 μs, and the delay time between the laser pulse Q-switch and the spectrometer detection was adapted to be 1 μs, which was considered as an optimum to reach the LTE plasma as found before [16].

3.　Result and Discussion

3.1.　Studies of LIBS Spectrum

The qualitative compositional analysis of the Cu target is achieved from the optical emission spectrum of the laser-produced plasma created on the target surface using the ultrafast picosecond Nd:YAG pulsed
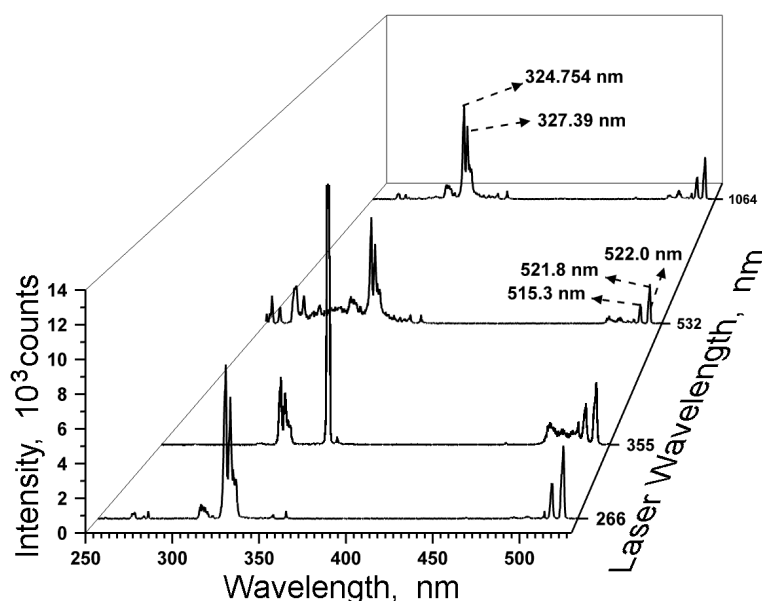
Fig. 1. LIBS emission spectra of Cu target generated by the laser pulse with an energy of 60 mJ at different laser wavelengths equal to 266, 355, 532, and 1064 nm.

laser.

Figure 1 represents the LIBS emission spectra of the Cu sample in the wavelength range $250-550$ nm at different laser wavelengths L_λ equal to 266, 355, 532, and 1064 nm. All the spectra were recorded under identical experimental conditions. This spectral region is selected to exploit a transparency of the optically thin LTE plasma of the parameters found previously [17]. The three selected lines of singly-ionized copper are Cu I lines (515.320, 521.820, and 522.007 nm) due to the transitions $(3d^{10}4d, {}^2D_{3/2} \rightarrow 3d^{10}4p, {}^2P_{1/2})$, $(3d^{10}4d, {}^2D_{5/2} \rightarrow 3d^{10}4p, {}^2P_{3/2})$, and $(3d^{10}4p, {}^2P_{3/2} \rightarrow 3d^{10}4d, {}^2D_{3/2})$, respectively. The characteristics and transitions of the selected Cu emission lines were identified with the help of the NIST database as shown in Table 1 with the data used to calculate the plasma electron temperature [18].

Table 1. Spectroscopic Parameters of the Emission Lines of Cu I Used to Calculate the Plasma Parameters Taken from the NIST Database [18].

Wavelength of Cu I nm	Transitions			Transition probability A_{ki}, 10^7 s^{-1}	Energies, eV			g_k
	Upper level		Lower level		E_k	E_i	ΔE	
515.320	$3d^{10}4d, 2D_{3/2}$	$\rightarrow$	$3d^{10}4p, {}^2P_{1/2}$	6.00	6.191	3.785	2.406	4
521.820	$3d^{10}4d, 2D_{5/2}$	$\rightarrow$	$3d^{10}4p, {}^2P_{3/2}$	7.50	6.192	3.816	2.376	6
522.007	$3d^{10}4p, {}^2P_{3/2}$	$\rightarrow$	$3d^{10}4d, {}^2D_{3/2}$	1.50	6.191	3.816	2.375	4

3.2. Plasma Electron Temperature and LTE Considerations

Under the assumed local thermodynamic equilibrium (LTE) condition, where the emissions from electron collisions are much larger than that from the radiative processes [19], the plasma temperature can be calculated from the emission-line intensities of Cu, applying the Boltzmann plot method [16,20,21]; the result is

$$I = FC \frac{A_{ki} g_k}{\lambda U(T)} \exp\left(-\frac{E_k}{KT_e}\right); \tag{1}$$

the natural logarithm of Eq. (1) reads

$$\ln \frac{I\lambda}{A_{ki} g_k} = -\frac{1}{KT_e} E_k + \ln \frac{FC}{U(T)} . \tag{2}$$

Here, I is the intensity of the spectral line, λ is the wavelength of the spectral line, K is the Boltzmann constant, $U(T)$ is the partition function, A_{ki} is the transition probability, g_k is the statistical weight for the upper level, E_k is the excited-level energy, T_e is the electron temperature, F is an experimental factor, and C is the concentration of species.

The Boltzmann plots for Cu I lines (515.32, 521.82, and 522.0 nm) at a laser pulse energy of 60 mJ are presented in Fig. 2, where the value $\ln \dfrac{I\lambda}{A_{ki} g_k}$ is considered for each exciting energy E_k at different $\lambda = 266, 355, 532,$ and 1064 nm. The electron temperature can be estimated from the slope provided by Eq. (2) with an uncertainty of about $\pm 8\%$, which mostly is related to the errors in measurements of the emission-line intensities and the transition probabilities [14,17]. The observed data from the Boltzmann plots are summarized in Table 2 with a linear correlation coefficient R^2 for each of the laser pulse energies.
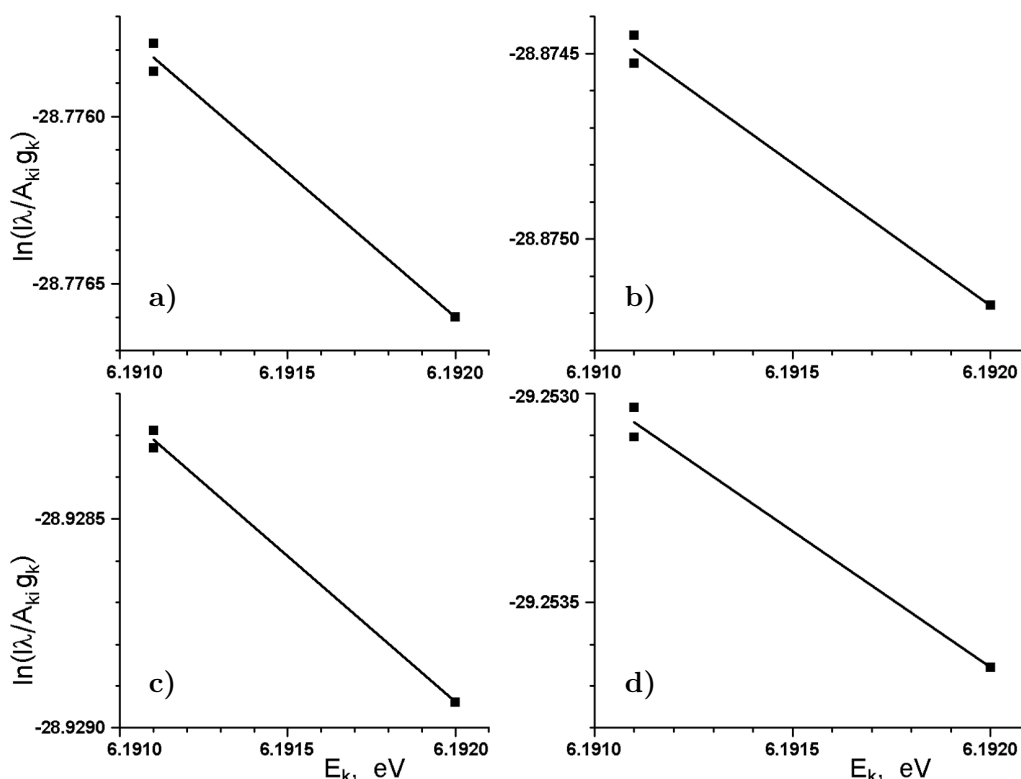
Fig. 2. Boltzmann plots for the Cu I lines (515.32, 521.82, and 522.0 nm) at a laser pulse energy of 60 mJ and laser wavelengths 266 nm (a), 355 nm (b), 532 nm (c), and 1064 nm (d).
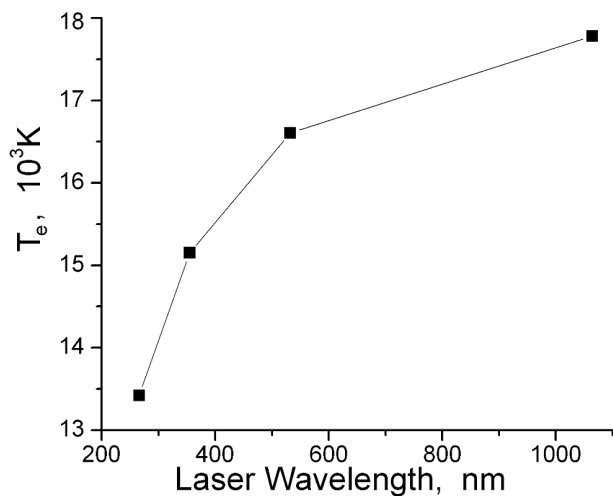
Fig. 3. The effect of different laser wavelengths and pulse energies on the Cu plasma temperature T_e.

Table 2. Data Analysis of the Boltzmann Plots and the Plasma Plume Temperature T_e at Different Laser Pulse Energies and Laser Wavelengths with Correlation Coefficient R^2.

Laser wavelength, nm	Slope	T_e, K	R^2
266	-0.8646	13422.3	0.992
355	-0.7659	15152.1	0.991
532	-0.6989	16604.6	0.996
1064	-0.6526	17782.7	0.989

From Table 2 we found that, at a laser pulse energy of 60 mJ, the plasma plume temperature ranges from around $13400\,\text{K}$ to $17800\,\text{K}$ depending on the laser wavelength.

Figure 3 demonstrates the dependence of the Cu plasma temperature on laser wavelengths at a laser pulse energy of 60 mJ. The plasma electron temperature increases with the laser wavelength, which is in

agreement with earlier studies [22,23]. This increase in the plasma temperature with the laser wavelength is related to plasma shielding [24, 25]. Due to the plasma shielding, once a plasma is generated, a part of the laser beam is absorbed by the plasma, by electron–ion inverse Bremsstrahlung or electron-neutral inverse Bremsstrahlung, and photoionization. The probability of electron–ion interaction is much higher than that of electron–neutral one, except at a very early stage of the laser evaporation process; according to this fact, electron–neutral inverse Bremsstrahlung is generally considered negligible during laser-induced plasma processes [23,24]. While, the inverse Bremsstrahlung absorption coefficient α_{IB} and the photoionization absorption coefficient α_{PI} are given in [26] as follows:

$$\alpha_{\text{IB}} = 1.37 \cdot 10^{-35} L_\lambda^3 N_e^2 T_e^{-1/2}, \tag{3}$$

$$\alpha_{\text{PI}} = 7.9 \cdot 10^{18} \left(\frac{L_\lambda E_n}{hc}\right)^3 \left(\frac{I}{E_n}\right)^{1/2} \sum_n N_{e_n}, \tag{4}$$

where L_λ is the laser wavelength in micrometers, T_e is the plasma electron temperature, E_n and N_{e_n} are the ionization energy and electron density of the excited state n, respectively, h is the Planck constant, c is the speed of light in vacuum, and I is the ionization potential of the atomic ground state.

The results obtained demonstrate that the plasma electron temperature is directly proportional to the laser wavelength L_λ at fixed laser pulse energy. This profile can be understood as follows: When laser interacts with the target surface, it creates plasma. The plasma near the focusing point is very hot and emits the Bremsstrahlung, known as the background emission.

Considering Eqs. (3) and (4), which depend on the laser wavelength, we can infer that the inverse Bremsstrahlung is the dominant interaction mechanism at 1064 nm (NIR), while the photoionization becomes the significant interaction mechanism at 266 nm (UV) [27,28]. Recently, Tan et al. have shown that for ultrafast picosecond laser pulse, the plasma shielding retains a great impact on the laser-induced plasma generation [10]. Increase in the laser wavelength from the UV to NIR leads to the increase in the target's surface temperature [29], which enhanced the number of free electrons. So, at 1064 nm (NIR), due to the inverse Bremsstrahlung, most of the laser energy is absorbed by free electrons of the target [10] that causes an increase in the electron temperature. These results are in agreement with the previous studies [10, 28, 30].

4.   Conclusions

In this work, we studied the influence of the ultrafast picosecond laser wavelength at constant laser pulse energy on the generated copper-plasma plume parameters using the LIBS technique. We perceived that the plasma temperature displayed a strong dependence on the laser wavelength. We considered both the inverse Bremsstrahlung and photoionization absorption mechanisms for shielding of the copper surface and plasma. Increase in the picosecond-laser wavelength improves the plasma shielding due to the inverse Bremsstrahlung as the main absorption mechanism over the photoionization. So, most of the laser energy would be absorbed by free electrons of the target and preserves more energetic electrons, i.e., an increase in the electron temperature is connected with the increase in the picosecond laser wavelength. The obtained results revealed that the plasma temperature could be varied from 13400 K to 17800 K by altering the ultrafast laser wavelength. This result can be applied for plasma interaction dynamics, which is substantial for plasma spectroscopy of material science applications.

References

1. A. S. Eddington, *The Internal Constitution of the Stars*, Cambridge University Press (1988).
2. B. R. Adhikari and R. Khanal, *Himal. Phys.*, **4**, 60 (2013).
3. U. Fantz, *Plasma Sources Sci. Technol.*, **15**, S137 (2006).
4. H. Conrads and M. Schmidt, *Plasma Sources Sci. Technol.*, **9**, 441 (2000).
5. T. L. Thiem, R. H. Salter, J. A. Gardner, et al., *Appl. Spectrosc.*, **48**, 58 (1994).
6. D. A. Rusak, B. C. Castle, B. W. Smith, et al., "Fundamentals and applications of laser-induced breakdown spectroscopy," in: *Crit. Rev. Anal. Chem.*, Taylor & Francis Group (1997), Vol. 27.
7. M. A. Gondal and M. A. Dastageer, "Elemental analysis of soils by laser-induced breakdown spectroscopy," in: *Springer Ser. Opt. Sci.* (2014), Vol. 182, p. 293.
8. A. Jarota, E. Pastorczak, W. Tawfik, et al., *Phys. Chem. Chem. Phys.*, **21**, 192 (2019).
9. K. C. Phillips, H. H. Gandhi, E. Mazur, et al., *Adv. Opt. Photon.*, **7**, 684 (2015).
10. S. Tan, J. Wu, Y. Zhang, et al., *Energies*, **11**, 3163 (2018).
11. G. Abdellatif and H. Imam, *Spectrochim. Acta B: At. Spectrosc.*, **57**, 1155 (2002).
12. L. Fornarini, V. Spizzichino, F. Colao, et al., *Anal. Bioanal. Chem.*, **385**, 272 (2006).
13. S. Messaoud Aberkane, A. Bendib, K. Yahiaoui, et al., *Spectrochim. Acta B: At. Spectrosc.*, **113**, 147 (2015).
14. W. Xu, A. Chen, Q. Wang, et al., *J. Anal. At. Spectrom.*, **34**, 1018 (2019).
15. W. A. Farooq, A. S. Al-Johani, M. S. Alsalhi, et al., *J. Mol. Struct.*, **1201**, 127152 (2020).
16. W. A. Farooq, W. Tawfik, F. N. Al-Mutairi, et al., *J. Korean Opt. Soc.*, **17**, 548 (2013).
17. R. Qindeel and W. Tawfik, *Optoelectron. Adv. Mater. Rapid Commun.*, **8**, 741 (2014).
18. A. Kramida, Y. Ralchenko, J. Reader, et al., Spectra Database (ver. 5.6.1) NIST At., National Institute of Standards and Technology, Gaithersburg, MD [http://physics.nist.gov/asd (2019)].
19. A. B. Gojani, *ISRN Spectrosc.*, **2012**, 1 (2012).
20. W. T. Y. Mohamed, *Opt. Appl.*, **37**, 5 (2007).
21. H. C. Liu, X. L. Mao, J. H. Yoo, et al., *Spectrochim. Acta B: At. Spectrosc.*, **54**, 1607 (1999).
22. J. Hoffman, T. Moscicki, and Z. Szymanski, *Appl. Phys. A: Mater. Sci. Process.*, **104**, 815 (2011).
23. A. E. Hussein, P. K. Diwakar, S. S. Harilal, et al., *J. Appl. Phys.*, **113**, 143305 (2013).
24. A. Bogaerts and Z. Chen, *Spectrochim. Acta B: At. Spectrosc.*, **60**, 1280 (2005).
25. L. M. Cabalin and J. J. Laserna, *Spectrochim. Acta B: At. Spectrosc.*, **53**, 723 (1998).
26. J. J. Chang and B. E. Warner, *Appl. Phys. Lett.*, **69**, 473 (1996).
27. X. L. Mao, O. V. Borisov, and R. E. Russo, *Spectrochim. Acta B: At. Spectrosc.*, **53**, 731 (1998).
28. J. S. Cowpe, R. D. Moorehead, D. Moser, et al., *Spectrochim. Acta B: At. Spectrosc.*, **66**, 290 (2011).
29. K. Afb, N'Mu, and M. Eluille Clark, NASA Technical Note, D-5311 (1969).
30. X. L. Mao, A. C. Ciocan, O. V. Borisov, et al., *Appl. Surf. Sci.*, **127**–**129**, 262 (1998).

Terms and Conditions

Springer Nature journal content, brought to you courtesy of Springer Nature Customer Service Center GmbH ("Springer Nature").

Springer Nature supports a reasonable amount of sharing of research papers by authors, subscribers and authorised users ("Users"), for small-scale personal, non-commercial use provided that all copyright, trade and service marks and other proprietary notices are maintained. By accessing, sharing, receiving or otherwise using the Springer Nature journal content you agree to these terms of use ("Terms"). For these purposes, Springer Nature considers academic use (by researchers and students) to be non-commercial.

These Terms are supplementary and will apply in addition to any applicable website terms and conditions, a relevant site licence or a personal subscription. These Terms will prevail over any conflict or ambiguity with regards to the relevant terms, a site licence or a personal subscription (to the extent of the conflict or ambiguity only). For Creative Commons-licensed articles, the terms of the Creative Commons license used will apply.

We collect and use personal data to provide access to the Springer Nature journal content. We may also use these personal data internally within ResearchGate and Springer Nature and as agreed share it, in an anonymised way, for purposes of tracking, analysis and reporting. We will not otherwise disclose your personal data outside the ResearchGate or the Springer Nature group of companies unless we have your permission as detailed in the Privacy Policy.

While Users may use the Springer Nature journal content for small scale, personal non-commercial use, it is important to note that Users may not:

1. use such content for the purpose of providing other users with access on a regular or large scale basis or as a means to circumvent access control;

2. use such content where to do so would be considered a criminal or statutory offence in any jurisdiction, or gives rise to civil liability, or is otherwise unlawful;

3. falsely or misleadingly imply or suggest endorsement, approval , sponsorship, or association unless explicitly agreed to by Springer Nature in writing;

4. use bots or other automated methods to access the content or redirect messages

5. override any security feature or exclusionary protocol; or

6. share the content in order to create substitute for Springer Nature products or services or a systematic database of Springer Nature journal content.

In line with the restriction against commercial use, Springer Nature does not permit the creation of a product or service that creates revenue, royalties, rent or income from our content or its inclusion as part of a paid for service or for other commercial gain. Springer Nature journal content cannot be used for inter-library loans and librarians may not upload Springer Nature journal content on a large scale into their, or any other, institutional repository.

These terms of use are reviewed regularly and may be amended at any time. Springer Nature is not obligated to publish any information or content on this website and may remove it or features or functionality at our sole discretion, at any time with or without notice. Springer Nature may revoke this licence to you at any time and remove access to any copies of the Springer Nature journal content which have been saved.

To the fullest extent permitted by law, Springer Nature makes no warranties, representations or guarantees to Users, either express or implied with respect to the Springer nature journal content and all parties disclaim and waive any implied warranties or warranties imposed by law, including merchantability or fitness for any particular purpose.

Please note that these rights do not automatically extend to content, data or other material published by Springer Nature that may be licensed from third parties.

If you would like to use or distribute our Springer Nature journal content to a wider audience or on a regular basis or in any other manner not expressly permitted by these Terms, please contact Springer Nature at

onlineservice@springernature.com